R-06-54

Using observations in deposition tunnels to avoid intersections with critical fractures in deposition holes

Raymond Munier, Svensk Kärnbränslehantering AB

April 2006

Svensk Kärnbränslehantering AB
Swedish Nuclear Fuel
and Waste Management Co
Box 5864
SE-102 40 Stockholm Sweden
Tel 08-459 84 00
+46 8 459 84 00
Fax 08-661 57 19
+46 8 661 57 19

ISSN 1402-3091
SKB Rapport R-06-54

Using observations in deposition tunnels to avoid intersections with critical fractures in deposition holes

Raymond Munier, Svensk Kärnbränslehantering AB

April 2006

Contents

1 Introduction

The integrity of the canister/buffer system can be jeopardised by earthquakes that occur in the vicinity of the repository. To avoid mechanical damage due to earthquakes, SKB has adopted the notion of respect distance which, according to /Munier and Hökmark 2004/, is defined as follows:

"The respect distance is the perpendicular distance from a deformation zone that defines the volume within which deposition of canisters is prohibited, due to anticipitated, future seismic effects on canister integrity."

The use of respect distance alone cannot, however, guarantee the integrity of the canister. There is a relation between the respect distance and the size of fractures that can be allowed to intersect the deposition holes. If a fracture is too large it might, when triggered by a nearby earthquake, host a slip exceeding the canister failure criterion, 10 cm with the current canister design /Börgesson et al. 2003/. Empirical and numerical studies have shown /Munier and Hökmark 2004/ that a fracture must have a radius exceeding 50 m to be able to host a maximum slip of 10 cm, using a respect distance of 100 m. The numerical methods have since developed to include fracture friction and recent studies /Fälth and Hökmark 2006/ has concluded that the size of acceptable fracture sizes in deposition holes can be increased to r = 75 m (100 m respect distance) and r = 150 m (200 m respect distance) respectively. A deposition hole not fulfilling these criteria will be rejected. We find it practical for the purposes of this report, to follow the terminology of /Munier and Hökmark 2004/, in which these fractures are termed "discriminating fracture".

The problem is that the size of a fracture can rarely, if ever, be measured. A simple and uncontroversial indicator for a fracture being large is if its intersection with a tunnel can be traced around the full perimeter of the tunnel face (Figure 1-1). Such fracture intersections are easy to observe and require no additional efforts than traditional fracture mapping.

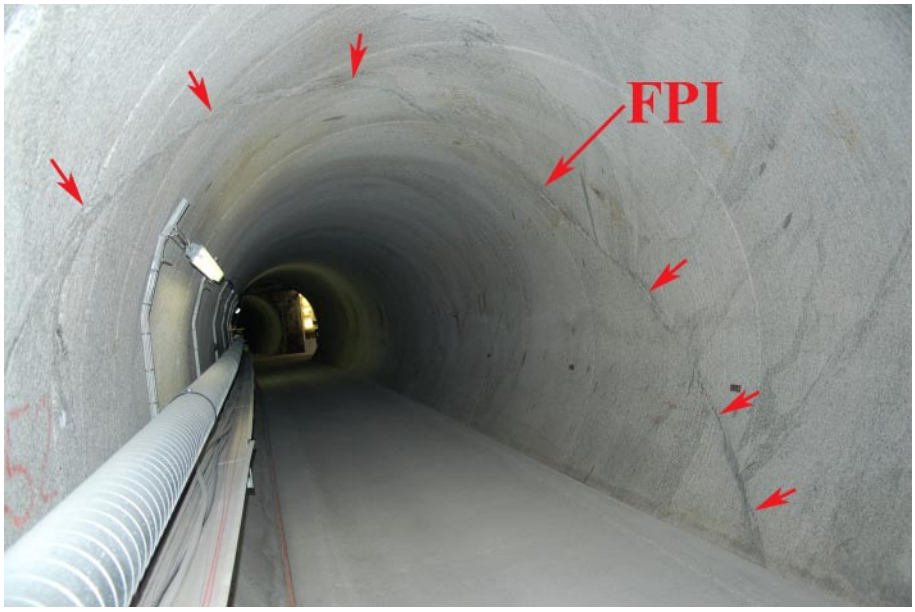

Figure 1-1. *Example of a full perimeter intersection, Grimsel test site, Switzerland.*

We here evaluate the efficiency of utilising a Full Perimeter Intersection (hereafter denoted FPI) criterion /e.g. Hagros et al. 2005/, for identifying discriminating fractures in deposition tunnels and deposition holes. We also evaluate the consequences of using FPI, expressed in terms of the degree of utilisation.

This is achieved by means of stochastic fracture simulation consisting of two steps. The first consists of computing intersection statistics between the tunnel and the fracture array. The second step consists of computing the degree of utilisation based on the statistics derived from the first step.

We base our simulations upon the DFN models produced for the Laxemar /Hermanson et al. 2005/ and Forsmark /La Pointe et al. 2005/ study sites, versions 1.2. We anticipate that these models will mature further within the framework of SKB's on-going site investigations and Site Modelling (versions 2.2 and onwards) and though we here discuss the impact of various DFN parameters on our results, it is beyond the scope of the work presented here to evaluate the validity of the published models. The DFN models have been used with no modifications and accepted as they were published. The uncertainties presented here thus mirror the uncertainties of the DFN models.

2 Simulation prerequisites

2.1 DFN model

The site descriptions /e.g. SKB 2005c/ and references therein provide the necessary fracture statistics to construct a DFN model. Here we make use of the Laxemar /Hermanson et al. 2005/ and Forsmark /La Pointe et al. 2005/ DFN versions 1.2, summarised and simplified in Table 2-1 and Table 2-2. A visualisation of the DFN models is displayed in Figure 2-1 as traces on a tentative outcrop which highlights the differences in fracture intensities between the sites.

Table 2-1. Laxemar DFN, version 1.2.

Mean orientation of fracture poles			Size		Intensity
Trend	Plunge	Kappa	k_r	r_0	P_{32}
338.1	4.5	13.06	2.85	0.328	1.310
100.4	0.2	19.62	3.04	0.977	1.026
212.9	0.9	10.46	3.01	0.858	0.975
3.3	62.1	10.13	4[1]	–	2.320
243.0	24.4	23.52	3.60[2]	0.400	1.400

[1] The distribution given by the DFN model is exponential with the parameter λ = 1/mean.
[2] As the Laxemar model did not report any parameters for the Euclidian scaling we used the reported fractal scaling instead.

Table 2-2. Forsmark DFN, version 1.2.

Mean orientation of fracture poles			Size		Intensity
Trend	Plunge	Kappa	k_r	r_0	P_{32}
87.2	1.7	21.66	2.88	0.28	0.602
135.2	2.7	21.54	3.02	0.25	2.069
40.6	2.2	23.9	2.81	0.14	0.448
190.4	0.7	30.63	2.95	0.15	0.226
342.9	80.3	8.18	2.92	0.25	0.605

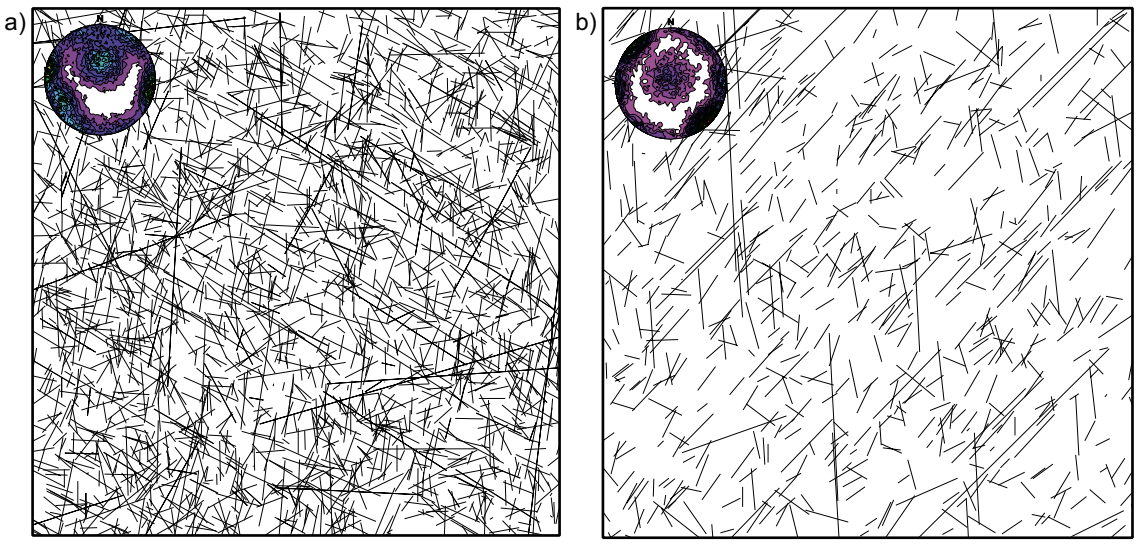

Figure 2-1. *DFN simulations of the size interval 1 < r < 250 m, here displayed as traces on a 50×50 m simulated outcrop. a) = Laxemar 1.2, b) = Forsmark 1.2. Inserts are contoured (Kamb) stereonets of poles to simulated fracture planes.*

2.2 Intersection criteria

In this study, we idealise a tunnel as a cylinder, and a fracture as an infinitely thin, circular disc. The problem studied here, is thus essentially one of finding the intersection between a finite plane and a finite cylinder.

There are many possible intersection geometries (Figure 2-2), all of which are discussed briefly below:

Intersection “b” is by far the most common and occurs when the plane intersects the cylinder at an oblique angle. Intersections “a” and “c” constitute special cases of “b” and occur when the plane is perpendicular or parallel to the cylinder respectively.

Intersection “d” requires the plane to be oriented exactly parallel to the tunnel, and located exactly at its tangent which is unlikely both in simulations and in a real tunnel system. The FPI criterion requires the fracture to be detectable by the naked eye and thus “d” type intersection will therefore not be included in the analyses. Intersections “f” and “g” are special cases of “d”.

Intersection “e” occurs if the fracture intersects the end-cap of the tunnel.

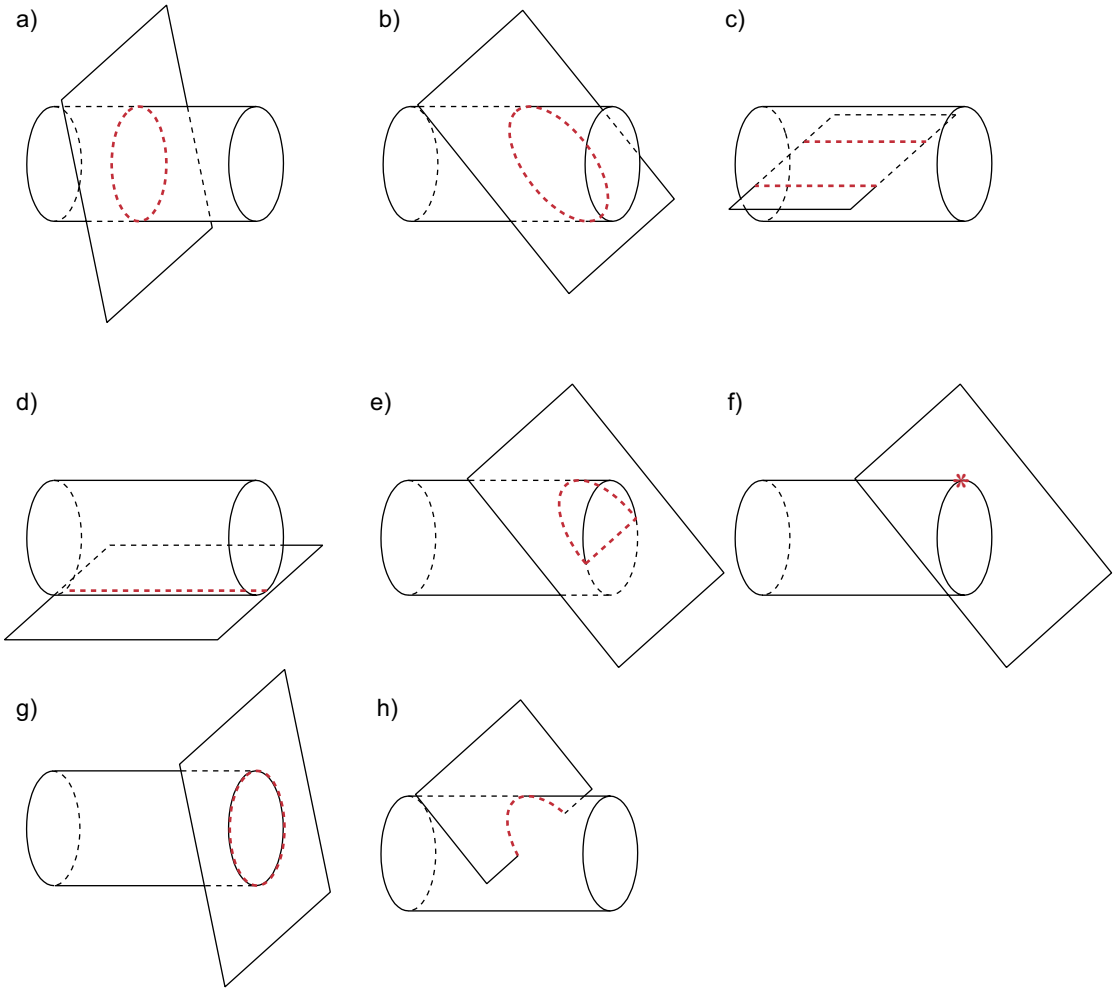

Figure 2-2. *Possible intersection geometries between an infinite plane and a finite cylinder (a–g). Possible intersection between a finite plane and a finite cylinder (h).*

In addition to the intersections above, we can envisage intersections as parts of ellipses (intersection “h”), which would occur if the planes were not large enough to cut through the entire tunnel diameter or located such that only the tip of the plane intersects. Such intersections are not relevant to our study. Thus, for the purpose of evaluating a FPI criterion, only intersections of type “a”, “b”, “c” and “e” were considered.

We define a plane P (Figure 2-3) in terms of its centre point, P_c, its unit vector, $\hat{n}$ and its radius r_p. A cylinder is defined in terms of its centre point C, its axis orientation, represented by the unit vector $\hat{c}$, its radius r_c and its half- length (or half- height) h.

If the plane is perpendicular to the cylinder, then the absolute value of the dot product equals one, i.e.:

$$\left| \hat{c} \cdot \hat{n} \right| = 1$$

and we will, for an *infinite* plane, have an intersection if the distance between P and C is less than or equal to h, producing an intersection of type “a” or “g” respectively.

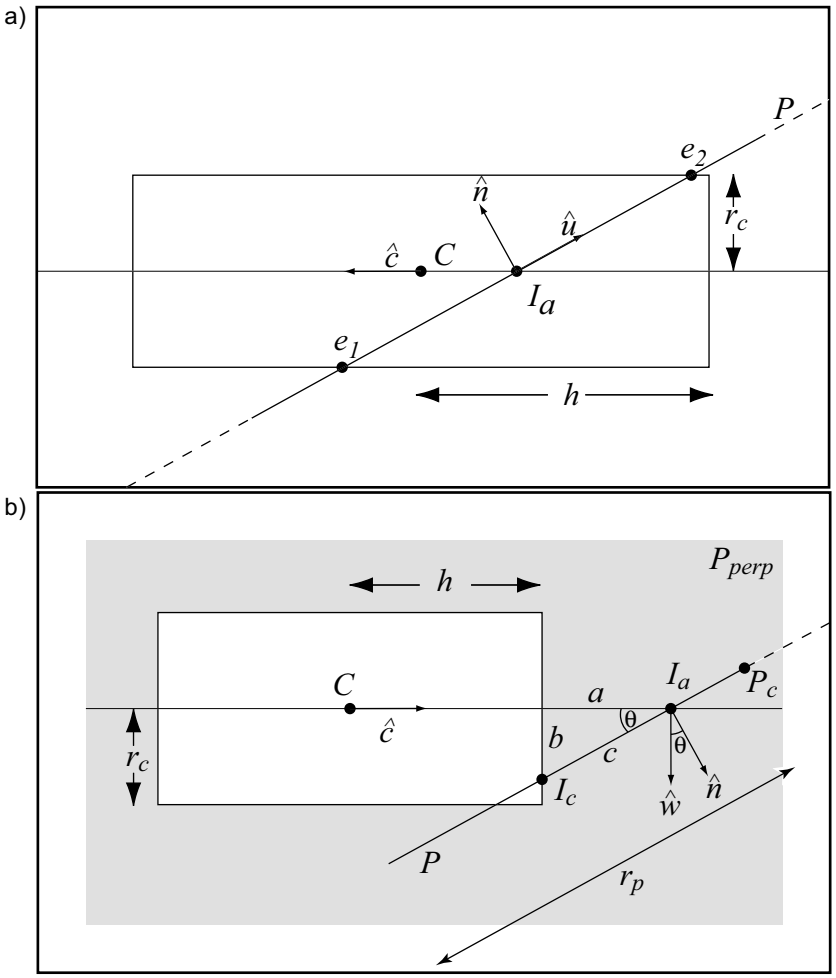

Figure 2-3. *a) Criteria for elliptical intersections. b) Criteria for end-cap intersections /redrawn from Schneider and Eberly 2003/.*

If the plane is parallel to the cylinder, the dot product is zero, i.e.:

$\hat{c} \cdot \hat{n} = 0$

and we will have an intersection if the distance between P and C is less than or equal to r_c producing type "c" or type "d" intersections, respectively.

If the plane is neither parallel nor perpendicular to the cylinder we have an intersection if the intersection point, I_a, between the plane and the cylinder axis is closer to C than the half length, h, which produces an intersection of type *"b"* or *"e" (or "h")*. However, the plane might intersect the axis beyond the end caps and there might be an intersection depending on the relative location and orientation of the objects. The intersection, if it does occur, will be of the types *"e"* or *"f"*.

To check for an intersections of type "*b*" we compute the intersection between the plane, the cylinder axis and the cylinder which produces an intersection point I_a and an ellipse (Figure 2-3a). Using the major axis of the ellipse, $\hat{u}$, we check if the ellipse, represented by the points e_1 and e_2, lie entirely within the end caps of the tunnel. If so, we have an intersection of type "b". If not, we may have an intersection of type "f" or "e". The latter, end-cap intersection, is computed as follows:

Following the reasoning in /Schneider and Eberly 2003. Section 11.7.3, pages 553–555./, for the case I_a lies beyond the end-caps (Figure 2-3b), we define a vector $\hat{w}$ such that:

$\hat{w} = \hat{c} \times (\hat{n} \times \hat{c})$, is a vector perpendicular to $\hat{c}$ that lies in the plane, P_{perp}, containing both $\hat{n}$ and $\hat{c}$ (see Figure 2-3b). That is, we can always compute intersections in a coordinate system perpendicular to the fracture plane because of the rotational symmetry of the cylinder.

The angle θ between $\hat{n}$ and $\hat{w}$ is:

$\cos(\theta) = \hat{n} \cdot \hat{w}$.

The distance a is known:

$a = \| I_a - C \| - h$

and by definition we know that:

$$\cos(\theta) = \frac{a}{c}.$$

Substituting, we get:

$$\hat{n} \cdot \hat{w} = \frac{\| I_a - C \| - h}{c}$$

and so

$$c = \frac{\| I_a - C \| - h}{\hat{n} \cdot \hat{w}}.$$

Since $a^2 + b^2 = c^2$, then

$$b^2 = \left(\frac{\| I_a - C \| - h}{\hat{n} \cdot \hat{w}} \right)^2 - \left(\| I_a - C \| - h \right)^2$$

If $b^2 \le r_c^2$ and $\| P_c - I_c \| \le r_p$ we have an intersection of type *"e"* (or *"f"*); otherwise, no intersection occurs.

3 Simulation procedure

We have implemented all simulations as Matlab /The MathWorks Inc 2006/ m-scripts, available from the author upon request. This section describes briefly the applied simulation principles.

3.1 Generation of fracture populations

The fractures in the DFN models used are assumed to possess a Poissonian spatial arrangement (i.e. non-correlated positions), and a lack of correlation between size, position and orientation within each defined fracture set. Simulation of a fracture population therefore constitutes no further complication than random sampling from the given distributions for each fracture set and joining all sets into a fracture population.

We made use of the inversion method /Devroye 1986/ to produce random numbers either using built-in routines in Matlab (applies to rectangular, exponential and lognormal distributions) or by the expressions below.

Hereafter denoting a [0, 1] sample from a uniform distribution as U, we obtain random numbers from a power-law distribution, r_{PL}, from:

$$r_{PL} = r_{min}\left[U\left(\left(\frac{r_{min}}{r_{max}}\right)^{k} - 1\right) + 1\right]^{-1/k} \qquad [1]$$

Similarly, random numbers from the univariate Fisher distribution can be obtained by three separate steps. We first sample the angular deviation from the mean poles, θ, using:

$$\theta = \arccos\left[\frac{1}{\kappa}\ln\left(e^{\kappa} - U\left(e^{\kappa} - e^{-\kappa}\right)\right)\right] \qquad [2]$$

These values can be regarded as the deviations from a vertical plunge (horizontal plane), i.e.

$$plunge = \frac{\pi}{2} - \theta$$

As the trend for a vertical plunge is uniform in [0, 2π], we obtain the trend from:

$$trend = 2\pi U$$

The set of vertical fracture normals thus produced is then rotated to the mean direction of the fracture set by first tilting the array to the mean plunge (i.e. rotation about a horizontal axis) and then adding the mean trend (i.e. rotation about a vertical axis).

The number of fractures N to be simulated is governed by the fracture intensity, P_{32}, provided by the DFN model. The intensity is defined as the fracture area per unit volume, and expressed in the unit m^2/m^3.

Following the reasoning in /Hedin 2005/, the number of fractures per unit volume, P_{30}, can be obtained from the relation:

$$P_{30} = n_0 f(r) \qquad [3]$$

where *f(r)* is the probability density distribution of fracture sizes for a particular fracture set. Unlike /Hedin 2005/, we use a *finite* model volume which tends to underestimate P_{32} because some portion of the simulated fracture will lie outside the finite model volume. This effect becomes smaller the larger the model volume (see Section 3.2). The factor n_0 is obtained from P_{32} through:

$$P_{32} = n_0 \pi \int_0^{\infty} r^2 f(r) dr \qquad [4]$$

Since we only simulate a portion of the population, *f(r)* in [3] must be integrated over the range (r_{min}, r_{max}). The number of fractures to simulate for each fracture set in a model volume, V, is then obtained by combining [3] and [4] into:

$$N = V \frac{P_{32}}{\pi \int_0^{\infty} r^2 f(r) dr} \int_{r_{min}}^{r_{max}} f(r)\, dr. \qquad [5]$$

To ensure homogeneous P_{32} throughout the model volume, in particular in the vicinity of the model boundaries, we implemented the fracture positions by sampling points randomly on the fracture surfaces, constraining the points to lie within the model volume. The procedure is described below.

A random point, P_r, is chosen from within the model volume as:

$$P_{rx} = Udx, \quad P_{ry} = Udy, \quad P_{rz} = Udz$$

where dx, dy and dz are the dimensions of the model volume in each principal direction respectively, and U is, again, a uniform random number in [0, 1]. The unit vectors parallel to the strike and dip directions, $\hat{s}$ and $\hat{d}$, respectively, are known. We rotate $\hat{s}$ randomly about P_r in the plane containing $\hat{s}$ and $\hat{d}$ using an angle:

$$\omega = 2\pi U.$$

The distance between P_r and P_c, $\| P_r - P_c \|$, is obtained from:

$$\| P_r - P_c \| = rU.$$

By trigonometry the centroid, P_c, can be obtained from:

$$P_c = P_r + \| P_r - P_c \| (\hat{s} \cos\omega + \hat{d} \sin\omega).$$

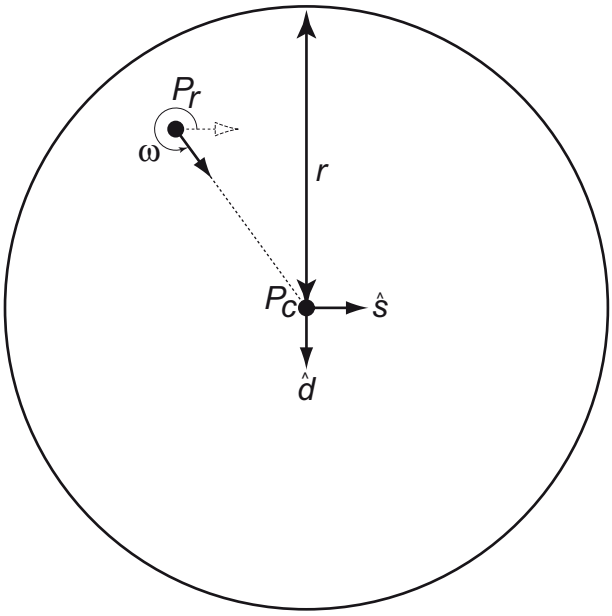

Figure 3-1. *Illustration showing the principle of deducing the fracture centroid from a randomly chosen point on the fracture surface.*

3.2 Choice of appropriate model volumes

Simulation of fractures honouring a specific intensity, P_{32}, requires the computation of fracture truncations against the boundaries of the model volume. This produces fractures of different shapes, each of which requires special handling, and is computationally expensive. To speed up simulations our procedures use P_{30}, the number of fractures per unit volume, to obtain required fracture intensity according to the input DFN model.

We do so by using equations [3]–[4] to transform P_{32} into P_{30}. This enables us to maintain the circular shape of the fractures and spares the routines from the burden of boundary intersection computations. The equations are, however, only valid for infinite volumes. There will always be a part of the fractures outside the finite model volume which do not contribute to P_{32}.

As the model volume increases, the fracture area outside the model volume will be increasingly smaller compared to the fracture area within the model volume. For a sufficiently large model volume, the difference can be regarded negligible. The size of the required volume is unknown, and is governed by both the DFN, mainly the size of the largest fracture to include, and the shape of the model volume.

As only fractures of radii up to a certain value, $r_{max,}$ are of interest for this study, the simple and absolute upper bound on the required model volume is dz = dy = $2(r_{max} + r_{Tunnel})$ and dx = $2r_{max} + L_{Tunnel}$. The use of such a large model results in very long computation times and shortage of computer memory. It is, however, possible to test for an appropriate volume by increasing the volume in steps until some test statistic, e.g. the number of FPI per 100 m, stabilises. The result of such a test is displayed in (Figure 3-2). The number of simulated FPI stabilises at model sides of approximately 150 m, for both Forsmark and Laxemar. Based on this analysis, we cautiously set the model side to 250 m, thereby decreasing both the model volume and computation time, by roughly a factor 6.

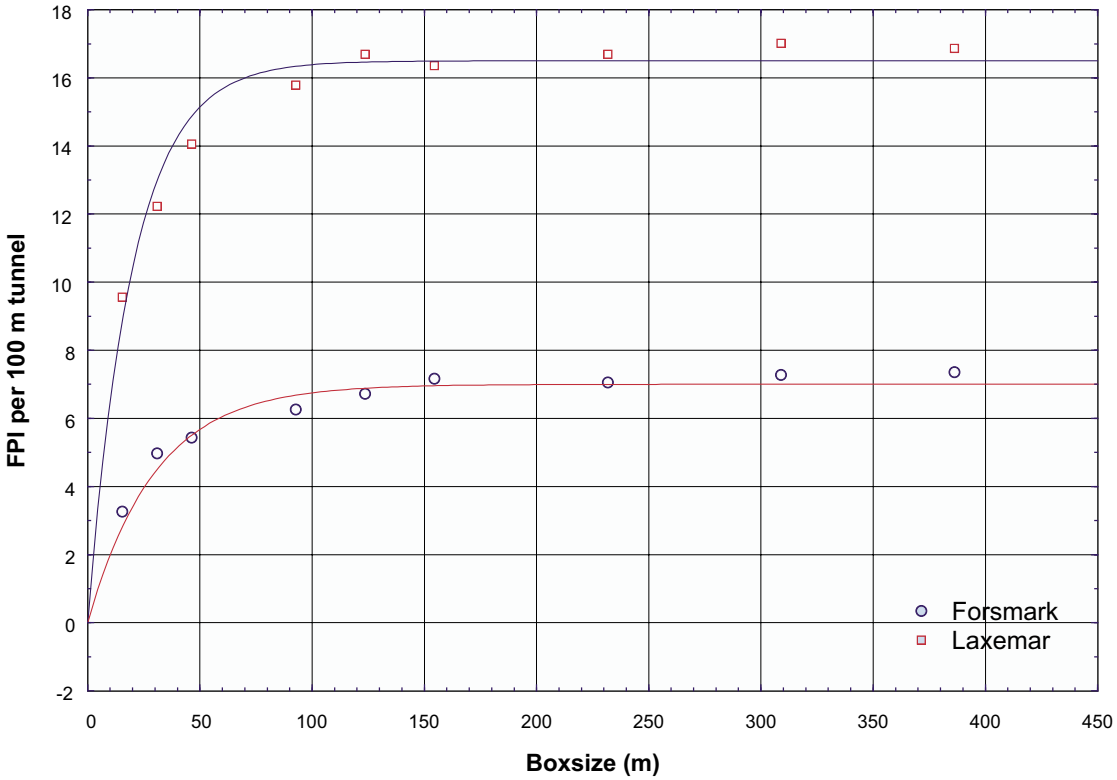

Figure 3-2. *Effect of model volume on intersection statistics. The computed FPI reaches a plateau at box sides of roughly 150 m.*

To increase simulation efficiency further, we made use of nested volumes, within which the resolution was made to differ (Figure 3-3), thereby dramatically decreasing the number of generated fractures which is the main factor governing computational speed. Additionally, we reduced the number of generated fractures by including only fractures equal to or exceeding the tunnel radius, which is required to produce an FPI. The fracture intensity has, naturally, to be rescaled to reflect the loss of small fractures. Furthermore, we presume that all fractures with radii exceeding r = 250 m, can be identified as minor deformation zones during tunnel mapping and hence can be safely excluded from the analyses. The tunnel length was set to 300 m, to reflect a realistic case, and its radius to 3.09 m, which corresponds to a cross-sectional area of 30 m^2 /SKB 2002/. The model volume was set to: dz = dy = 250 m, dx = 550 m.

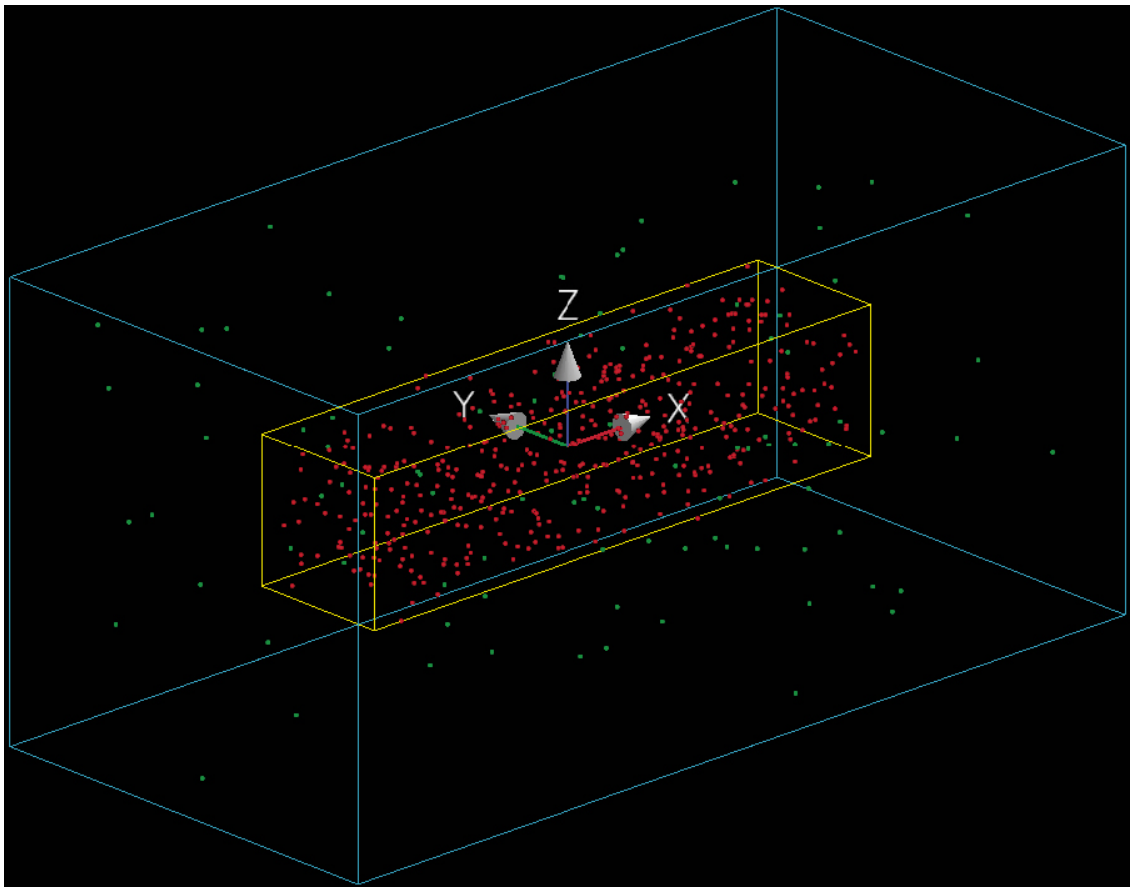

Figure 3-3. *Schematic figure showing the concept of nested volumes with fractures here represented by their centroids. Note that both the inner and outer boxes shown here are for illustration purposes only and are not drawn to scale.*

3.3 Computation of FPI

For computational convenience, we first compute the intersection between an infinite cylinder (the tunnel) and an infinite plane (the fracture). We then perform two tests to determine whether:

i) The intersection (both points e_1 and e_2 in Figure 2-3a) lies within the end-caps of the cylinder and

ii) The distance between the intersection (both points e_1 and e_2 in Figure 2-3a) and the plane centre is smaller than or equal to the plane radius.

For each realisation, we mark all simulated fractures that produce FPIs, keeping all other parameters such as location, orientation and size intact. This enables us to compute various detailed statistics on the intersecting fractures.

3.4 Choice of the appropriate number of realisations

We computed cumulative means and cumulative standard deviations for both the number of FPIs and degree of utilisation (explained below) which were used as measures to address the required number of realisations. An example is shown in Figure 3-4, using the Laxemar DFN and an EW trending tunnel. The mean and standard deviation of the number of FPI, as successively averaged over the realisations, stabilises after approximately 100 realisations.

To evaluate the impact of tunnel orientation on the computations, we rotated the tunnel 180° from East to West in steps of 10°. However, rather than rotating the tunnel itself, we mimicked tunnel rotation by rotating the fracture array, as this was found more computationally efficient. The required number of realisations is found to be dependent on tunnel orientation but the difference is subordinate and 500 realisations were found to be sufficient to ensure adequately small confidence intervals of the means.

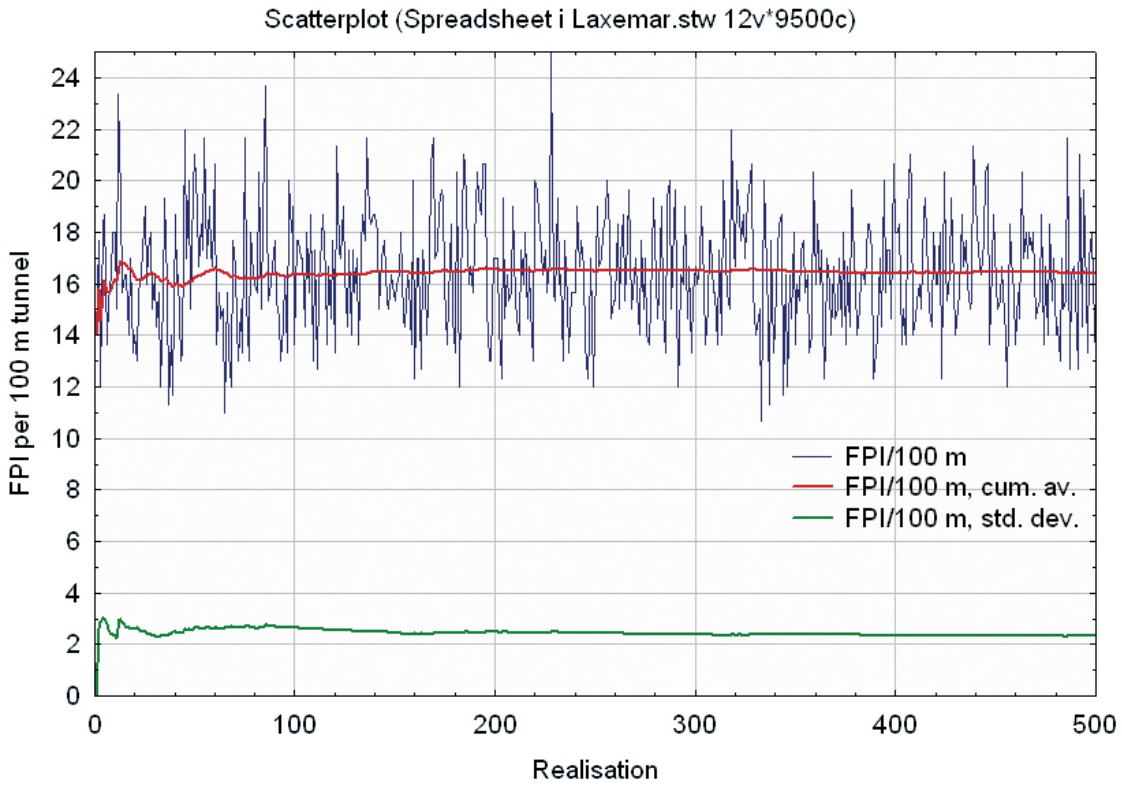

Figure 3-4. *The mean number of FPI per 100 m tunnel stabilises after about 100 realisations.*

4 Evaluation of Full Perimeter Intersections

Using the Laxemar DFN, the number of FPI varies with tunnel orientations between about 14 and 17 per 100 m of tunnel, Figure 4-1. The dependence on tunnel orientation is slightly more accentuated when using the Forsmark DFN, Figure 4-2, though the number of FPI per 100 m tunnel is lower and varies between approximately 4 and 8.

The noticeable difference between the two sites can be mainly attributed to the difference in P_{32} and r_0. (Table 2-1 and Table 2-2). Note that the subhorizontal Laxemar set hardly contributes to simulations, as very few sufficiently large fractures are generated for the exponential size distribution. In the studied radius range 3.09–250 m, the fracture intensity at Laxemar is about 2.4 times larger than at Forsmark, despite the lack of contribution to P_{32} of the subhorizontal set. The Laxemar and Forsmark DFN have approximately the same k_r as averaged over all fracture sets (2.97 and 2.92 respectively) but differ by a factor 3 in r_0 (0.64 and 0.21 respectively). The effect of a larger r_0 is that relatively more of the larger fractures are produced, everything else held equal. Since the largest fractures are those most likely to produce FPIs, we conclude that the difference in intersection statistics can be attributed mainly to the differences in P_{32} combined with, to a lesser extent, the differences in r_0.

The computed number of FPIs agrees well with approximate analytical solutions which were derived (Hedin 2006, personal communication) by following the principles outlined for canister intersections in /Hedin 2005/. Strict lower and upper bounds were obtained and these are shown in Figure 4-1 and Figure 4-2.

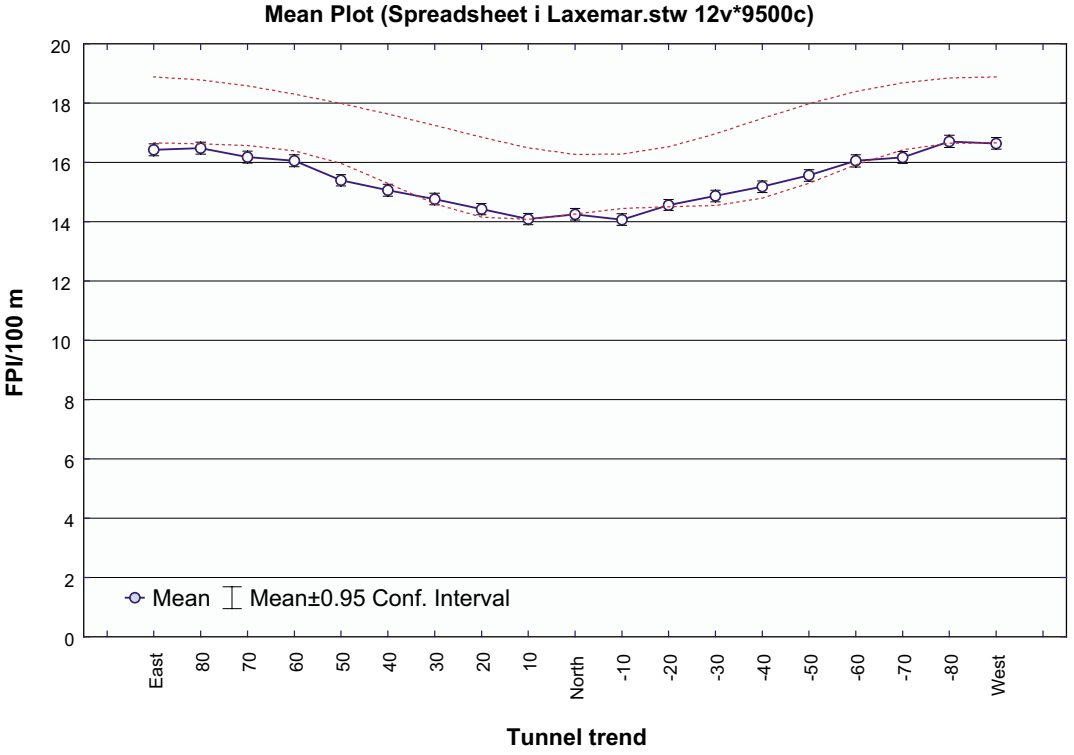

Figure 4-1. *Number of FPI per 100 m tunnel as a function of tunnel orientation (Laxemar 1.2). Dashed lines represent minimum and maximum number of FPI according to the analytical solution.*

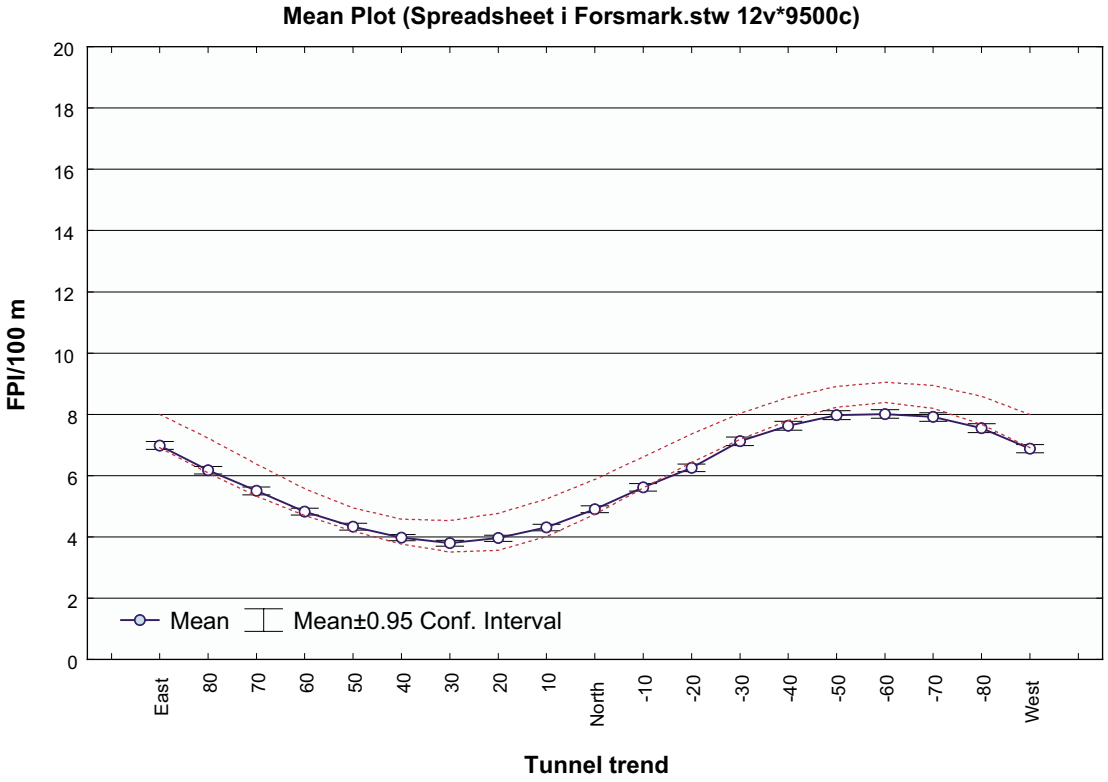

Figure 4-2. *Number of FPI per 100 m tunnel as a function of tunnel orientation (Forsmark 1.2). Dashed lines represent minimum and maximum number of FPI according to the analytical solution.*

5 The Full Perimeter Criterion

5.1 Definition

As stated above, the main objective of this work is to evaluate the possibility of using an easily identifiable characteristic of fractures, the Full Perimeter Intersection (FPI), to identify traces of large fractures in a *tunnel*. The ultimate goal is, however, to evaluate if FPIs can be used to identify *deposition holes* intersected by fractures large enough to constitute a seismic hazard.

We choose to do so by introducing the full perimeter criterion, FPC. Applying the FPC means that the (infinite) extrapolation of the earlier defined FPI (Figure 5-1) is used to represent a fracture of unknown size. Any deposition hole intersected by such extrapolation will be considered for rejection regardless of the true fracture size.

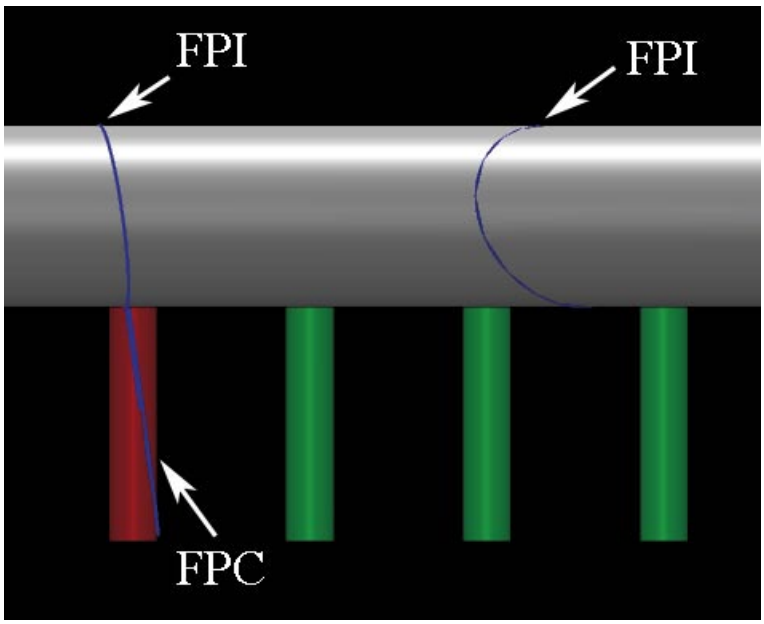

Figure 5-1. *The FPI mapped in the tunnel is judged to represent the trace of a discriminating fracture if its projection intersects the deposition hole.*

5.2 Need for an expanded FPC

There is a complication, though, in that the FPC fails to detect all discriminating fractures. For instance, it is likely that large fractures that do not intersect the deposition tunnel but are sufficiently close, have the potential to intersect a relatively large number of deposition holes (Figure 5-2), thereby further decreasing the degree of utilisation (see Chapter 6 for definition).

By analogy with the rationale for using the FPC, the size of these fractures will be unknown and we would need a similar criterion.

One criterion that could be used is the number of deposition holes across which the fracture can be traced. There will be a balance between the ability to trace the fracture across multiple deposition holes with confidence, and the acceptable degree of utilisation.

Figure 5-3 shows a plan view of a deposition tunnel, and a subhorizontal fracture of size "r" cutting through 5 deposition holes. The radius of a fracture that encircles exactly 5 deposition holes is denoted "r'". If it is reasonable to assume that a fracture can be confidently traced across, say, 5 deposition holes, the radius of the discriminating fracture is at least 0.5x (4×6) = 12 m. More generally, if we denote the number of intersected position as "n'", and the standard distance between canisters as "D" then:

$$r' = \frac{1}{2} D\left(n' - 1\right). \qquad [6]$$

Some fractures will escape detection despite this criterion. It is, for instance, possible for an r > 50 m fracture to intersect fewer than five deposition holes if it is located near the edge of the tunnel (e.g. Figure 5-4). It is also possible, though less likely, that deposition holes are intersected close to the fracture tip. Both these effects can be taken into account by using a stricter criterion, e.g., using two intersections or more (rather than 5 or more) as the criterion, at the expense of the degree of utilisation (See Section 6.2 for details). The expanded FPC will hereafter be referred to as "EFPC" and, if not stated differently, will be composed of both FPC and the contribution of the so expanded criterion.

Figure 5-2. *A potentially discriminating fracture can remain undetected despite the use of the full perimeter criterion in the deposition tunnel.*

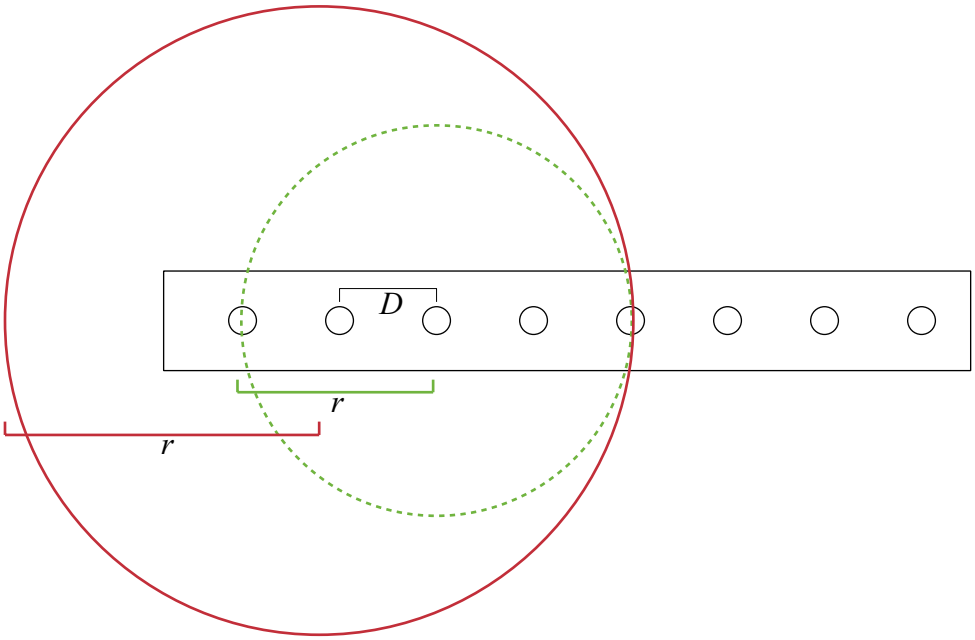

Figure 5-3. *Additional rejection criterion.*

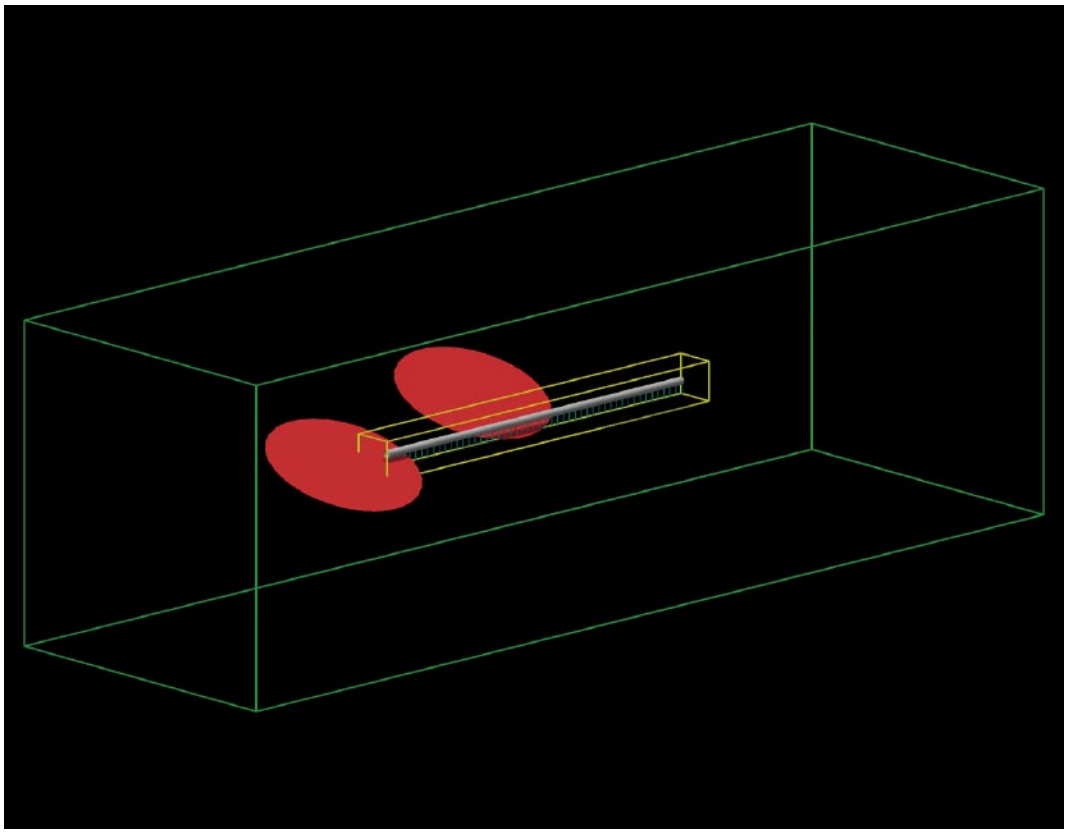

Figure 5-4. *The figure illustrates two cases for which the expanded FPC (EFPC) fails to detect discriminating fractures.*

5.3 Efficiencies of the criteria

An important question to address is how efficient the proposed criteria are in detecting the supposedly discriminating fractures. For this analysis, we restricted the number of simulations to 150 for each tunnel orientation, i.e. a total of 2,850 realisations (19 tunnel rotations), to obtain a manageable computation time and size of output.

We may regard each realisation as an equally possible, 300 m long, deposition tunnel randomly chosen from a repository layout. The spacing of deposition holes is, in the base case, 6 m. Consequence calculations should, according to SKB, be based on 6,000 canisters (the actual number, for which a license application will be made, will be determined at a later time). 2,850 realisations would correspond to 23.75 "repositories" (142,500 canisters).

Table 5-1 shows the number of simulated fractures, intersecting deposition holes, and having 50 m radius or larger that were not detected with either of the criteria (see e.g. Figure 5-4 for geometry), and the number of intersected deposition holes used as limit for EFPC. The total number of deposition holes intersected by undetected, discriminating fracture is 938 for all realisations. Normalised to a single, 6,000 canister large repository, the number of deposition holes is reduced to 40, or roughly 0.67%. That is, in a typical repository, 40 deposition holes will be intersected by discriminating fractures which would remain undetected by both criteria. The number of undetected and discriminating fractures decreases with fracture size as shown in Table 5-2.

We can express an efficiency of the applied criteria by comparing the results of the simulations presented here, to the number of intersections with deposition holes calculated analytically /Hedin 2005/ assuming no rejection criterion, which was used for the preliminary safety evaluations /SKB 2005ab/.

Table 5-2 shows that the application of FPC and EFPC aid in detecting a substantial amount of deposition holes intersected by discriminating fractures. For the currently computed, largest acceptable fracture radii in deposition holes, r = 75 m (100 m respect distance) and r = 150 m (200 m respect distance) /Fälth and Hökmark 2006/, the use of the criteria aid in detecting 94% and 97% of the affected deposition holes respectively.

Similarly, the efficiency of the applied criteria using the Laxemar DFN is shown in Table 5-3.

We accentuate, however, that only intersections with the *canisters* are of relevance for the safety assessments /e.g. SKB 2005ab/. As the intersection probability is lower for canisters than for deposition holes, due to the canisters smaller dimensions (r = 0.525 m, h = 4.83 m), the number of affected deposition holes will be lower than expressed in Table 5-2 and Table 5-3. Additionally, as the outermost portion of each fracture is unable to impose a threat to the canister integrity /see Hedin 2005 for discussion/, the number of affected deposition holes is further decreased.

Table 5-1. Number of canisters not detected by either of the criteria, using r = 50 m as the limit for a fracture to be regarded discriminating.

Intersected dep. holes per fracture	Number of fractures	Dep. holes
1	413	413
2	103	206
3	49	147
4	43	172
Sum	608	938

Table 5-2. Comparison of the use of criteria (FPC + EFPC) and "blind" deposition. Figures for blind deposition were computed according to the method given in /Hedin 2005/ using the dimensions of a deposition hole (r = 0.875 m, h = 7.833 m) and the full fracture area. Forsmark 1.2, 6,000 deposition hole layout.

	FPC + EFPC		"Blind" deposition		
Fracture radius	%	Number of deposition holes	%	Number of deposition holes	Efficiency of criteria (%)
≥ 50	0.66	40	7.56	454	91
≥ 75	0.26	16	4.50	270	94
≥ 100	0.13	8	2.93	176	96
≥ 150	0.04	2	1.33	80	97

Table 5-3. Comparison of the use of criteria and "blind" deposition. Figures for blind deposition were computed according to the method given in /Hedin 2005/ using the dimensions of a deposition hole (r = 0.875 m, h = 7.833 m) and the full fracture area. Laxemar 1.2, 6,000 deposition hole layout.

	FPC + EFPC		"Blind" deposition		
Fracture radius	%	Number of deposition holes	%	Number of deposition holes	Efficiency of criteria (%)
≥ 50	1.60	96	13.92	835	89
≥ 75	0.33	20	8.17	490	96
≥ 100	0.11	6	5.28	317	98
≥ 150	0.02	1	2.37	142	99

5.3.1 Varying criteria within the repository

According to /Fälth and Hökmark 2006/, the size of discriminating fracture can be set to 75 m in deposition holes located between 100 and 200 m from the deformation zone boundary and set to 150 m elsewhere in the repository.

Applying the findings of our simulations (Table 5-2) to the Forsmark layout, implies for instance, that if an earthquake of magnitude ≥ 6 would occur in the zone hosting the largest number of canisters within the 100 to 200 m band (the zone ZFMNE0060 with 563 such positions), see Figure 5-5, this would threaten less than 4 (563×0.26% + 5,437×0.04%) canisters remaining in unfavourable positions after application of the EFPC.

In Laxemar, the zone ZSMEW007A (Figure 5-6) is the one that affects the largest number of deposition holes (693). Applying the findings of our simulations (Table 5-3) to the Laxemar layout, implies that roughly 3 (693×0.33% + 5,307×0.02%) unfavourable canister positions will remain undetected using EFPC.

We again accentuate, however, that the reasoning here also assumes that the discriminating fractures are completely anonymous, displaying no geological information whatsoever that might reveal their size.

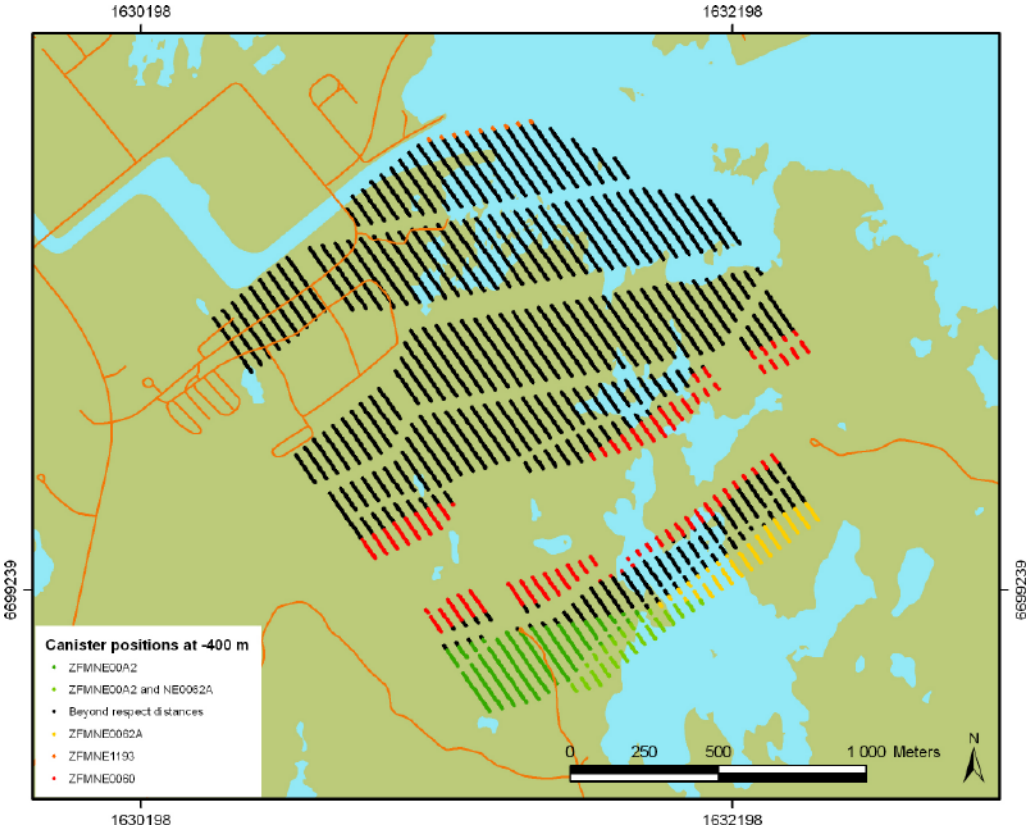

Figure 5-5. *The figure shows deposition tunnel sections with canister positions within a band positioned 100–200 m from deformation zones (Forsmark).*

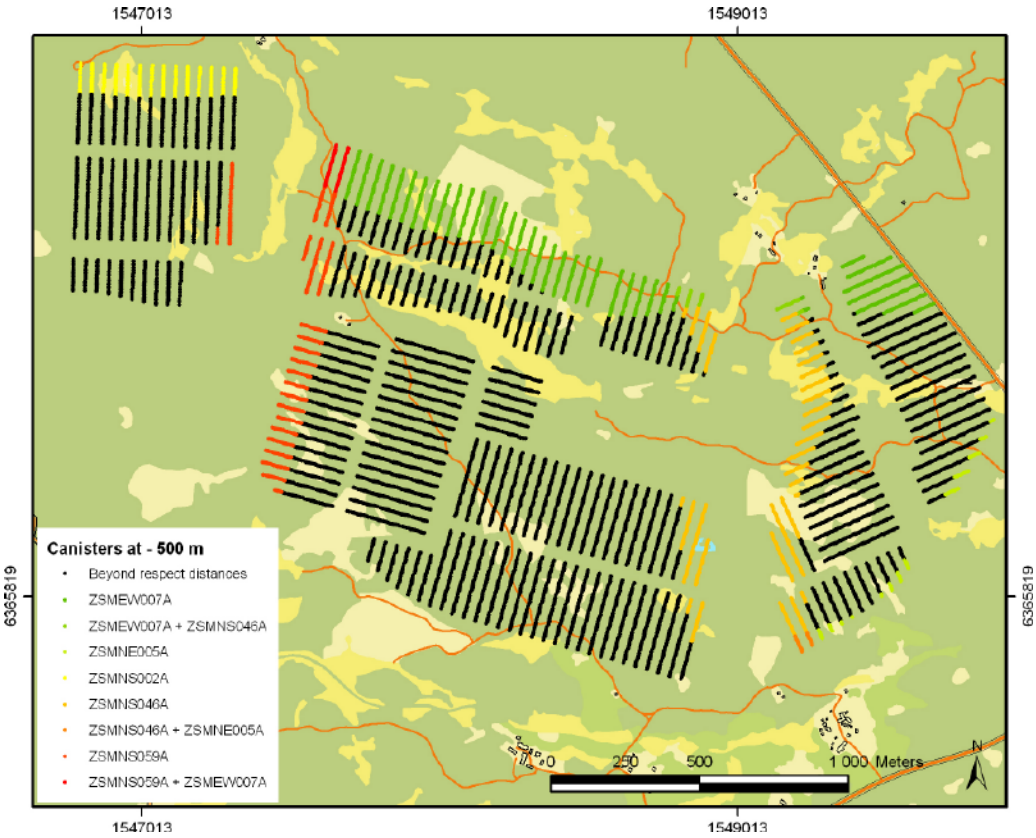

Figure 5-6. *The figure shows deposition tunnel sections with canister positions within a band positioned 100–200 m from deformation zones (Laxemar).*

5.3.2 Fracture size

The mean fracture radius is, expectedly, largest for fractures contributed by the expansion of FPC to EFPC (Figure 5-7). For the FPC alone, approximately 86% of the fractures indicated as potentially discriminating have radii smaller than 50 m, and approximately 96% have radii smaller than 100 m. For the contribution of EFPC, 78% of the fractures marked as discriminating have radii smaller than 50 m and 94% have radii smaller than 100 m. The size distributions for the fractures contributed by EFPC are shown in Figure 5-8.

5.3.3 Types of intersections

We computed the number of intersections of different types that were produced during simulations of all tunnel orientations. As expected, fractures producing the elliptical intersection, type “b”, dominate (Table 5-4). End cap intersections (type “e”) are more rare, constituting roughly 2.7% of all intersections.

It is noticeable that very few fractures, approximately 1.2% of all simulated, contributed to EFPC.

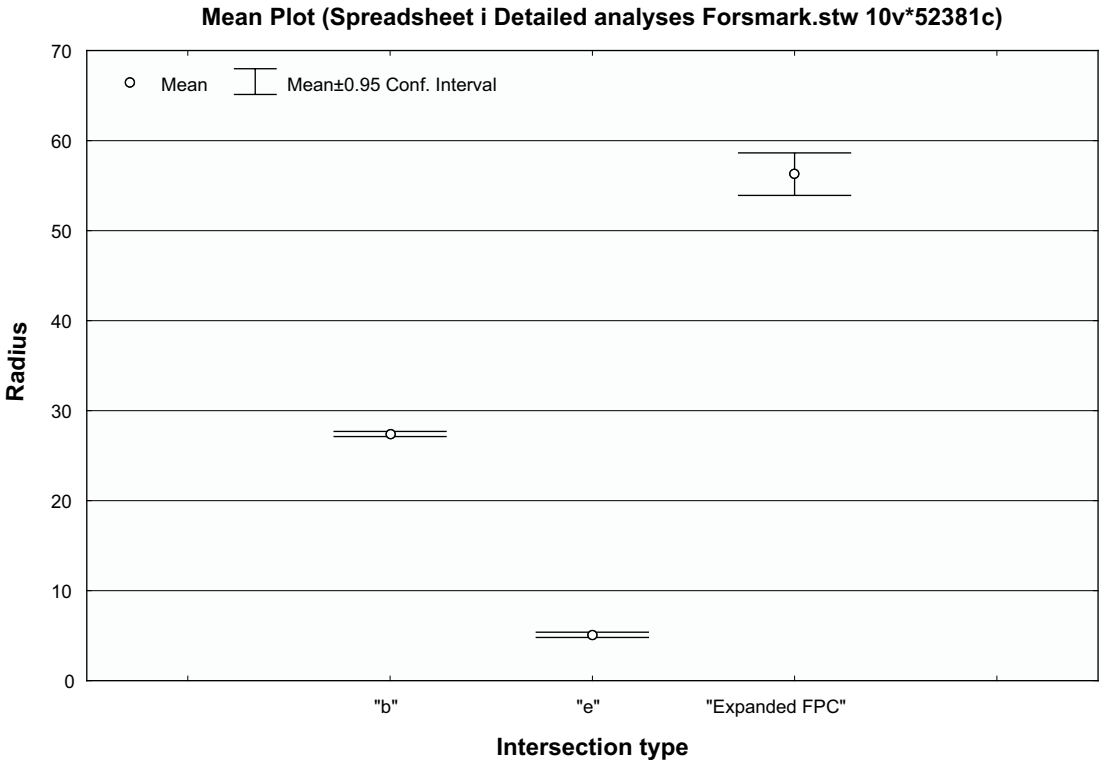

Figure 5-7. *Mean fracture radius for various intersection types at Forsmark.*

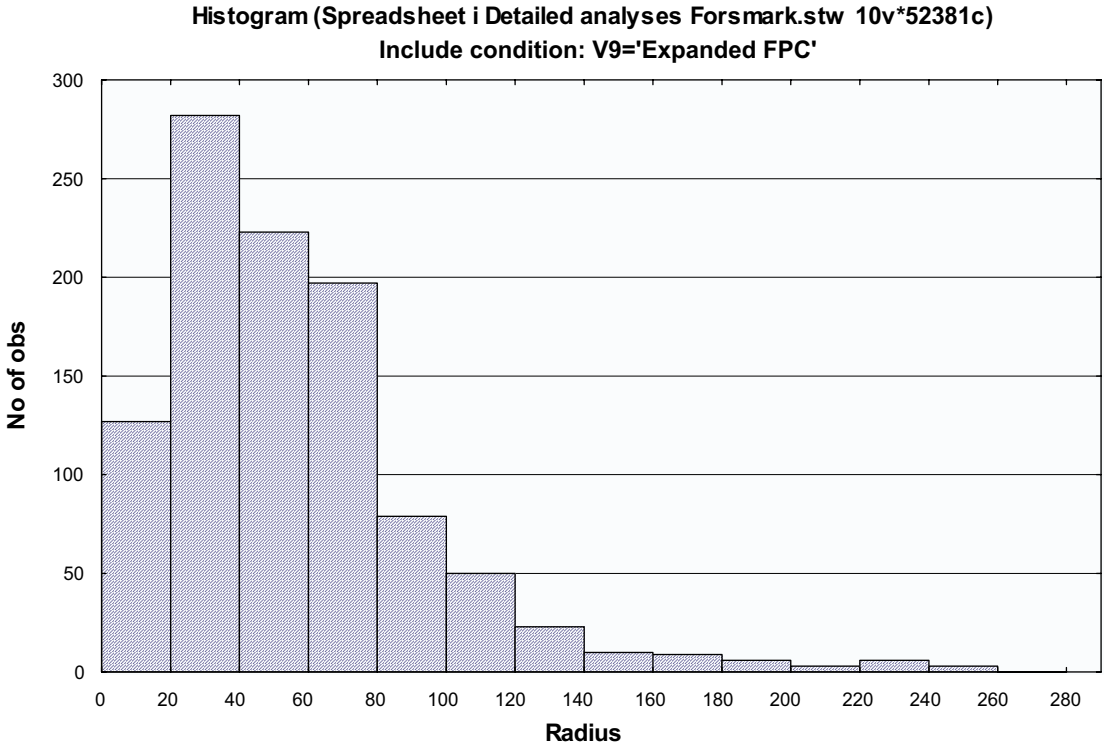

Figure 5-8. *Histograms of fracture radii for EFPC at Forsmark.*

Table 5-4. Summary of intersection types obtained for a simulation of Forsmark DFN, using all tunnel orientations and 150 realisations.

	Count	Cum. Count	Percent	Cum. Percent
Ellipse intersection (type “b”)	49,771	49,771	96.13312	96.1331
End cap intersection (type “e”)	1,396	51,167	2.69639	98.8295
Two lines intersection (Type “c”)	1	51,168	0.00193	98.8314
Intersection by Expanded criterion	605	51,773	1.16856	100.0000

6 Consequences of using FPC

6.1 Definition and model approach

In this section we explore the consequences of applying the FPC and expanded FPC in terms of the degree of utilisation. This entity, expressed in %, is defined as follows:

$$100 \times \frac{\text{Number of accepted positions}}{\text{Planned number of positions}} \% \qquad [7]$$

As the number of canisters to emplace is fixed, any degree of utilisation less than 100% must be compensated for by increasing the length of the deposition tunnel. In other words, the degree of utilisation is a measure of the required space for the repository.

For these simulations, we used the output from the simulations described in Chapter 4. The principles of the simulations are as follows:

Starting from the position of the first deposition hole, we try all FPI fractures for potential intersection. If none intersects, the position is accepted and a new position is tested a standard-distance *D* away. If, however, the position is intersected, we move the position until the fracture no longer intersects (Figure 6-1). For computational convenience we implement this reasoning in the codes by moving a small distance *d* and test all fractures again. The latter step is repeated until either the position is accepted or the end of the tunnel is reached. Note that, for this study, we used only the axes of deposition holes for

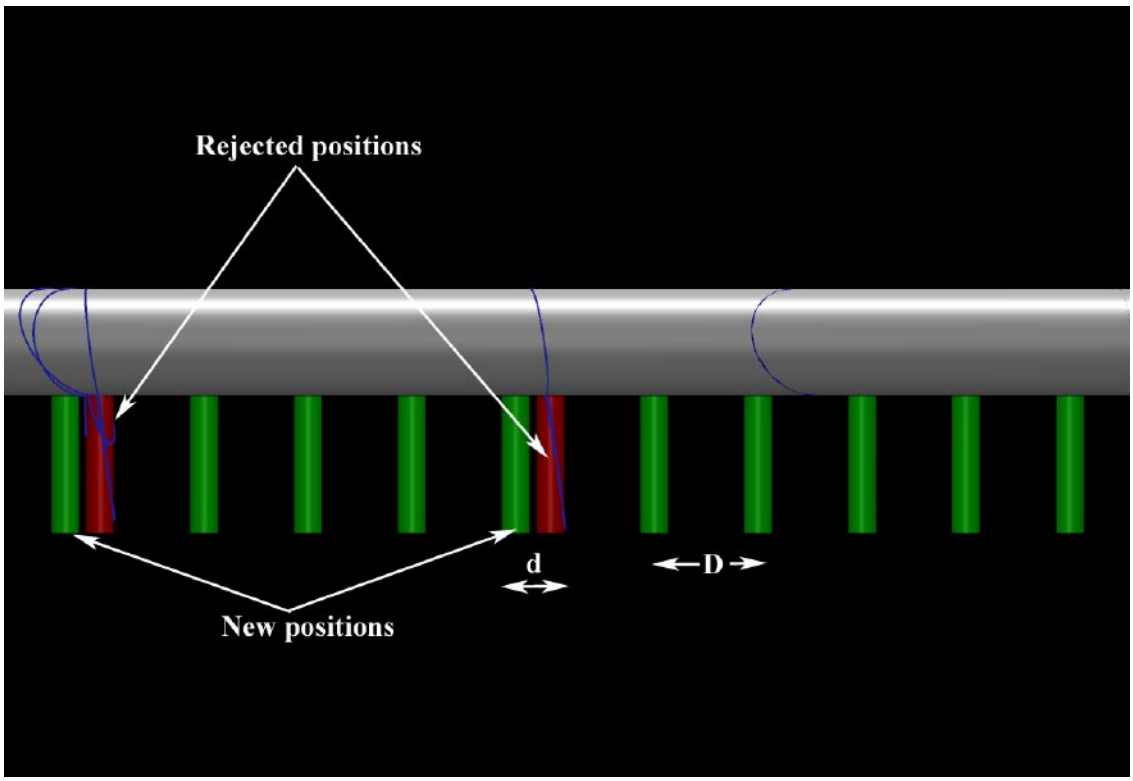

Figure 6-1. *Principles for simulating the degree of utilisation.*

the intersection tests. The use of cylinders with a diameter of the deposition holes will certainly increase the intersection probability but we do not anticipate any dramatic differences in results.

The standard-distance, D, is governed by, among other factors, the thermal properties of the rock /SKB 2004/. We used D = 6 m as our base case. The distance "d" should be as small as possible but there will be a trade off between optimisation and computation speed. We found d = 1 m appropriate for the purpose of the simulations presented here.

In the following sections we present results for Forsmark and Laxemar using 500 realisations for each tunnel direction. The large amount of realisations was judged necessary to demonstrate any potential difference between tunnel directions with statistical significance.

6.2 Degree of utilisation

6.2.1 Laxemar

The degree of utilisation for Laxemar, using FPC alone, varies with tunnel orientation between 87% and 89% when averaged over all realisations (Figure 6-2). Using EFPC, the degrees of utilisation are slightly lower and vary between 86% and 88%. Note, however, that it is almost impossible to differentiate between the two criteria for most tunnel orientations.

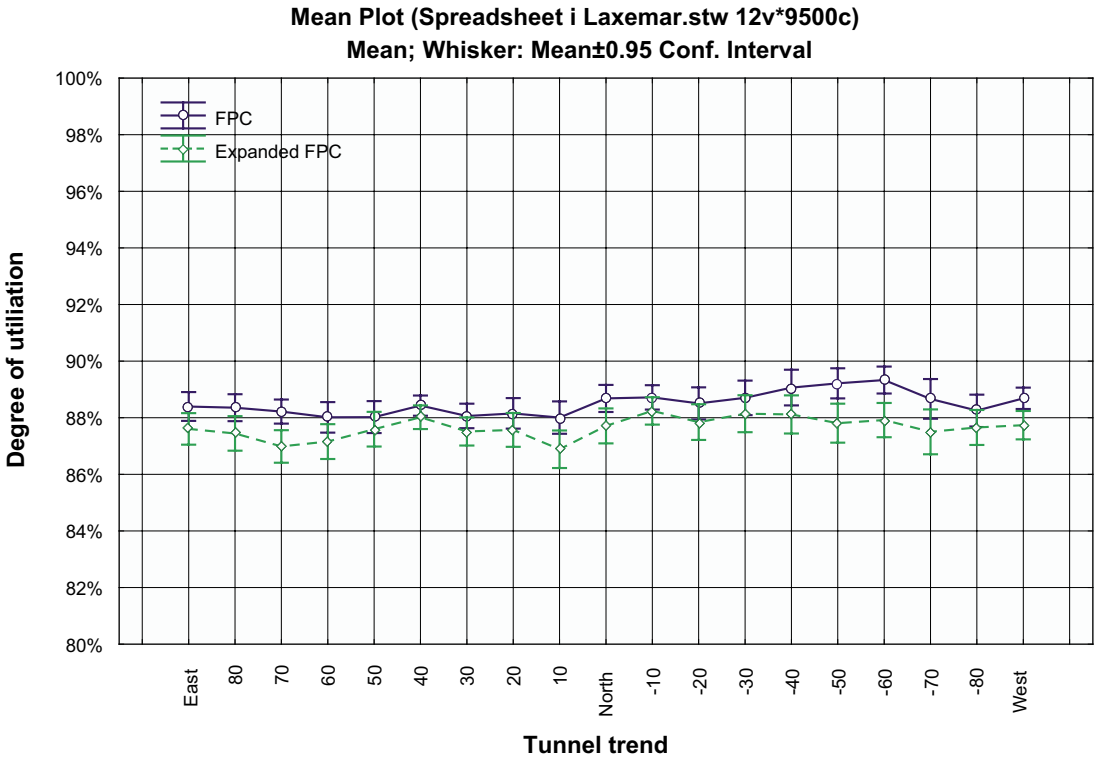

Figure 6-2. *Degree of utilisation as a function of tunnel orientation, Laxemar 1.2.*

6.2.2 Forsmark

The degree of utilisation for Forsmark, using FPC alone, is found to be weakly dependent on the tunnel orientation and varies between 93% and almost 95% (Figure 6-3) averaged over all realisations. Using EFPC, the degree of utilisation is noticeably lower and varies between 91% and 92%.

It can be seen in Figure 6-2 and Figure 6-3 that, for some tunnel orientations, the degree of utilisation is markedly lower than for others. These anomalies can be explained by the geometry of the fracture network. When the tunnel is parallel to any of the steep fracture sets for some realisations, a large number of deposition holes are affected by "chance". This is mainly because of the small dispersion in orientation, manifested as a large κ value, and the relatively large r_0, which tend to produce large fractures for some sets.

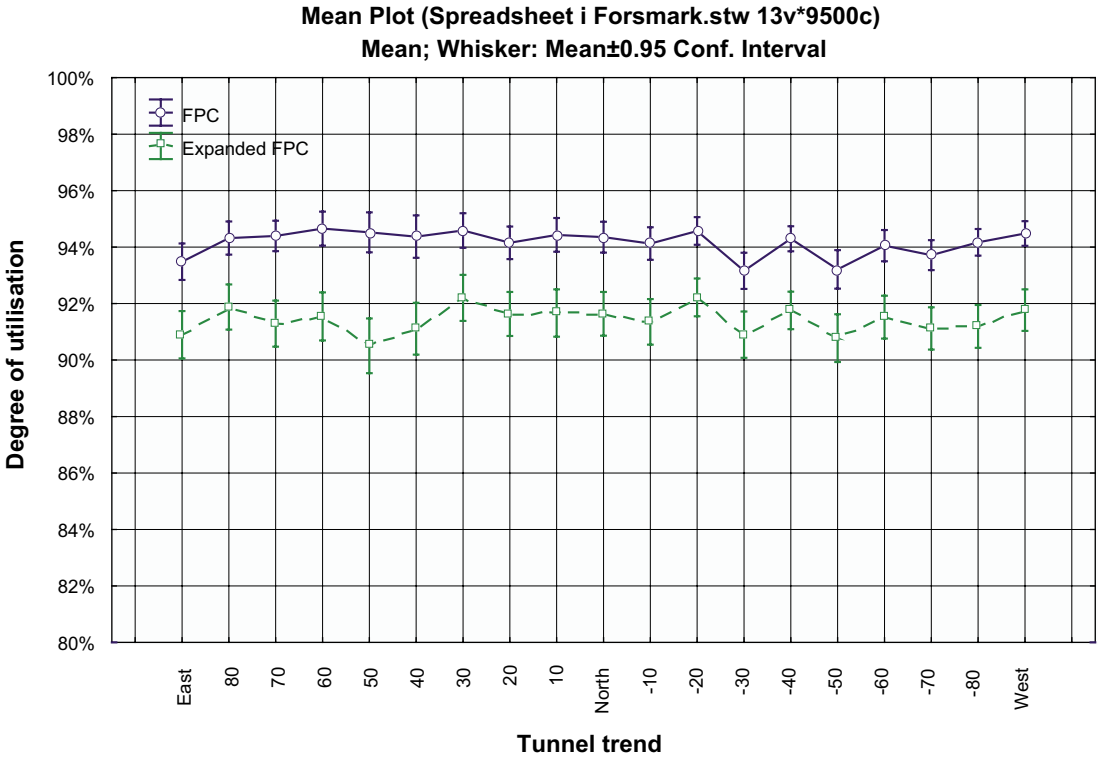

Figure 6-3. *Degree of utilisation as a function of tunnel orientation, Forsmark 1.2.*

6.3 Comparing FPC to EFPC

The contribution of EFPC to the degree of utilisation is illustrated in Figure 6-4. The diagram shows clearly that EFPC does not contribute significantly to the degree of utilisation for the vast majority, 7,719 out of a total of 9,500, of the realisations. However, the diagram also shows that for some realisations the contribution is significant, making up almost half of the loss of positions. As clearly shown in Figure 6-3 the difference in the results obtained between using FPC and EFPC, is caused by the relatively few realisations in which some large fractures with strikes sub-parallel to the deposition tunnels, have crosscut a large number of canister positions.

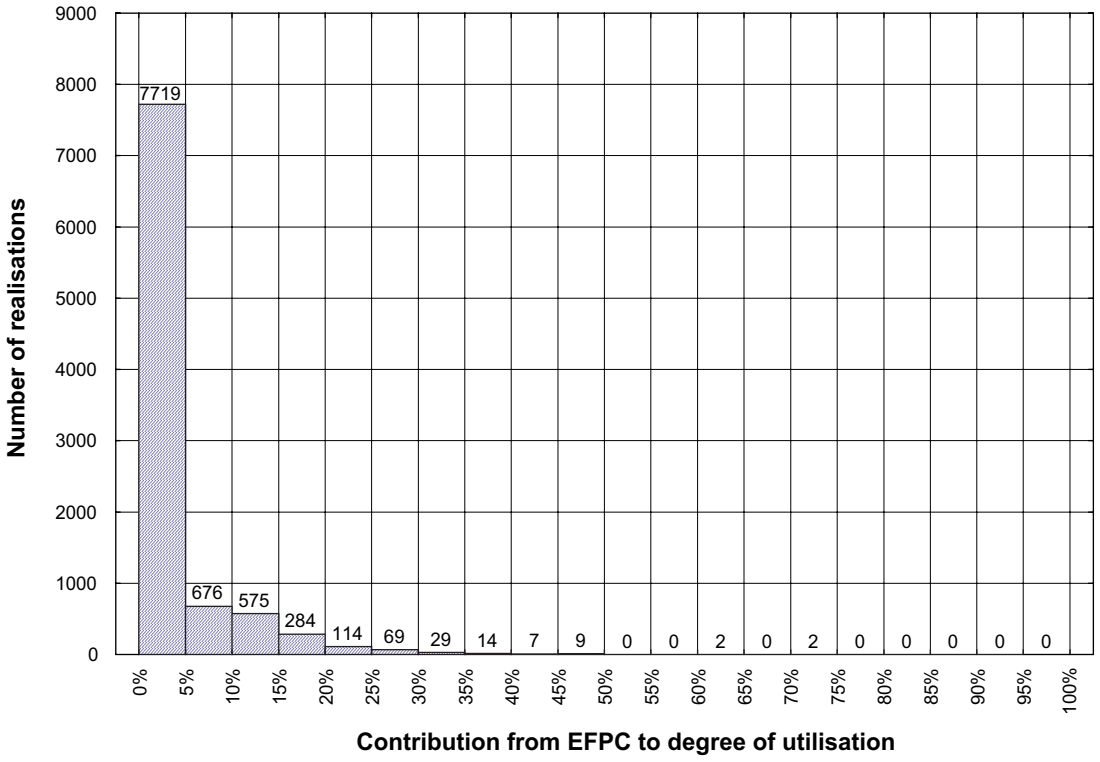

Figure 6-4. *Histograms showing the relative contribution of EFPC to the degree of utilisation.*

7 Sensitivity analyses

7.1 Difference between realisations

The difference can be very large between realisations due to the stochastic approach of the computations, but the results also differ largely between the Forsmark and Laxemar DFN. A lesson learned is that the test statistic must be chosen with care, when determining a sufficient amount of realisations for stability in the simulations. We initially used the number of FPI fractures/100 m as the simplest test statistic, which stabilised after relatively few realisations (ca 100, see Figure 3-4). However, using the same simulated data, computation of other statistics such as the confidence interval of the means required far more realisations to produce reliable results. We found, by trial, 500 realisations to be an appropriate amount for comparing FPC to EFPC. When the number of realisations increases, the confidence interval of the means decreases, rendering differences between e.g. tunnel orientations more statistically accentuated. Also by trial, we found 150 realisations to be an adequate number of realisations to evaluate the efficiency of the criteria. However, as a by-effect, the *range* of the outcome increases.

To illustrate the concept, we display the range of simulation outcome for the Laxemar DFN in Figure 7-1 and detailed in Figure 7-2. The lowest utilisation ratio of all realisations is 0%, which occurred at 4 out of 9,500 realisations (500 realisations times 19 tunnel orientations).

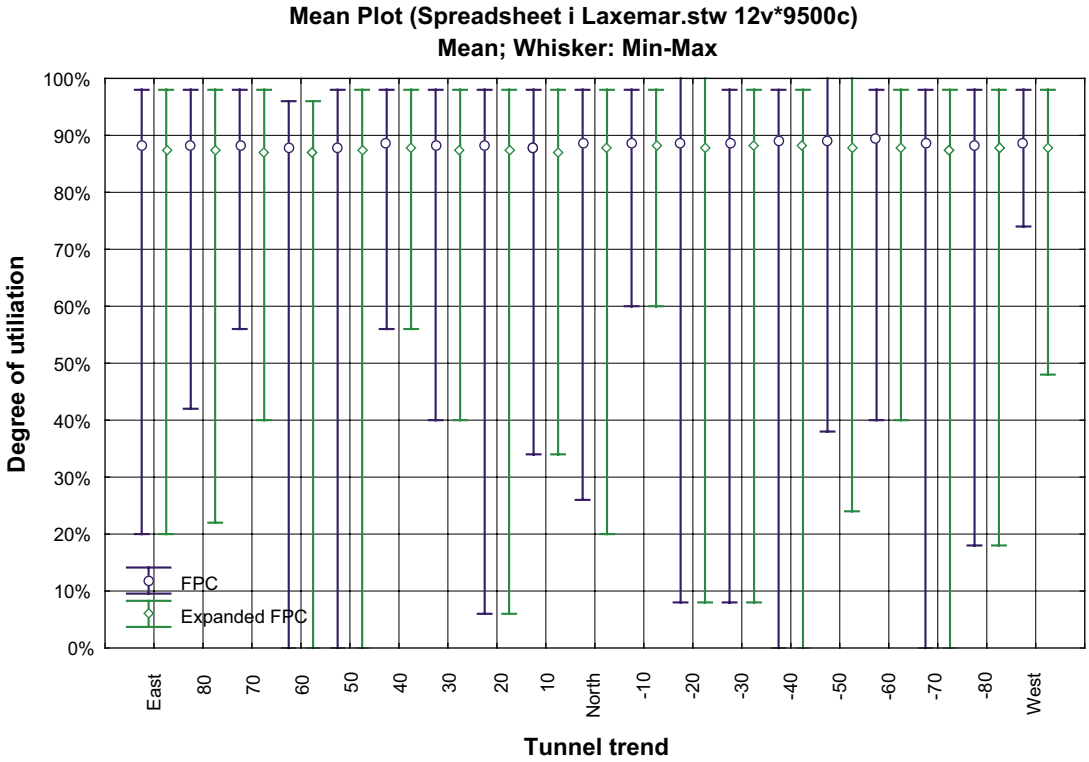

Figure 7-1. *Variability between realisations grouped by tunnel orientations, Laxemar 1.2. For clarity, the boxes are slightly offset on each side of the tunnel directions.*

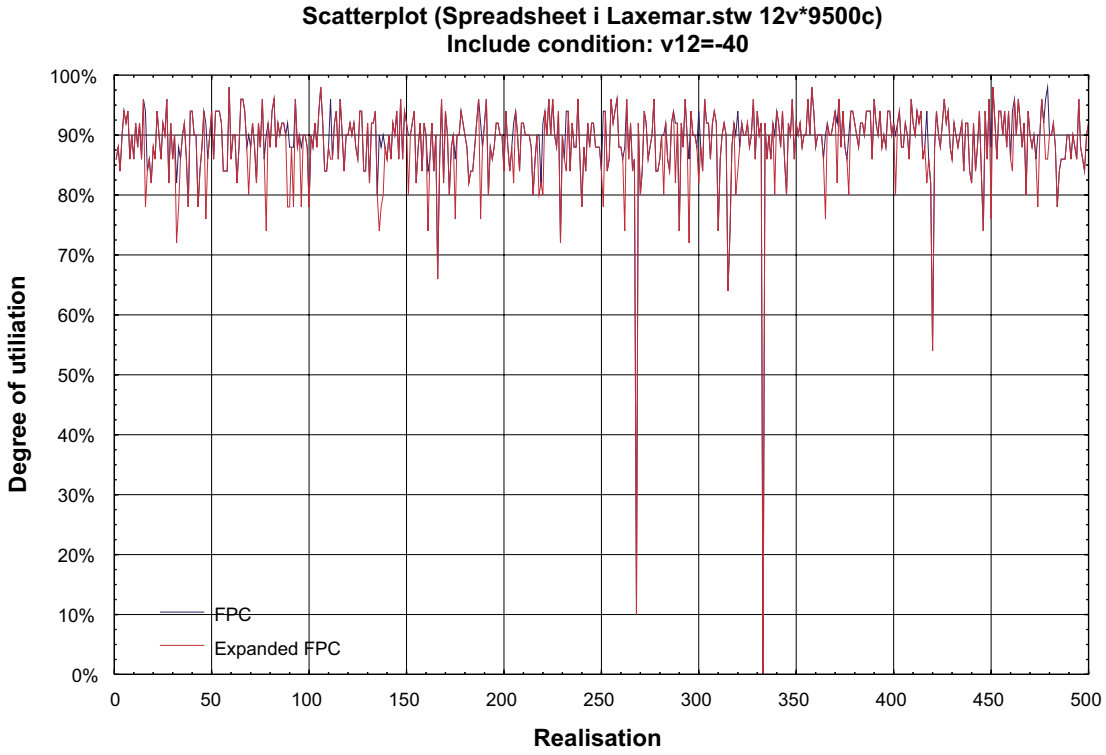

Figure 7-2. *Variability between realisations grouped for a tunnel oriented 320 (–40 in Figure 7-1), Laxemar 1.2.*

This should be interpreted the following way: 9,500 realisations of 300 m long tunnels, containing 50 canister positions each, correspond to 475,000 canister positions. This in turn corresponds to roughly 80 complete repositories containing 6,000 canisters each. Out of these 80 repositories, we anticipate 4 tunnels to be discriminated for deposition. In other words, there is a possibility that an entire tunnel will be discriminated, but the probability for this to occur is remote.

The 0% degree of utilisation occur when a realisation produces a few, large and essentially horizontal fractures. Many such fractures can probably be detected in probing boreholes, and the tunnel position can be moved an appropriate distance. Hence, in a real situation, this effect should not have such a dramatic impact on the degree of utilisation.

7.2 The effect of r’

We expanded FPC to discriminate also fractures that intersect 5 canister positions or more (see Section 5.2). This limit was arbitrarily chosen and, certainly, the choice of limit will steer the relative impact of EFPC upon the degree of utilisation. Using 5 canister positions, the minimum fracture radius to test, r’, is 12 m (cf equation [6]), of which there are relatively few. Besides, most fractures of this size are anticipated to possess some identifiable characteristic revealing their relative size, and more so, the larger the fracture. On the other hand, an anonymous fracture is probably very hard to trace over such distances in a normally fractured rock mass. This can be overcome by using fewer intersections for the criteria but that would decrease the degree of utilisation.

In Figure 7-3 we display the difference in degree of utilisation using different limits of EFPC, using the same batch of simulations as used for Figure 6-4. We increased the limit in steps from 2 canister intersections per fracture or more to 6 intersections or more. Naturally, as the limit increases, the degree of utilisation for EFPC approaches the degree of utilisation for the FPC because fewer fractures will meet the criterion due to the power-law size distribution.

In Table 7-1 we list the benefit of using a more restrictive limit for the EFPC. By discriminating fractures that intersect 2 deposition holes or more, we increase, to the cost of a lower degree of utilisation, the detection ratio from 91% (using 5 intersections) to 97%. Note that the efficiencies listed in Table 7-1 concern fractures of radii $r \geq 50$ m. For larger fractures, the efficiency is much higher.

Table 7-1. Efficiency of criteria using different limits on EFPC ($r \geq 50$ m).

Number of intersection in EFPC	Missed canisters	Efficiency
2	15	97%
3	23	95%
4	26	94%
5	39	91%
6	45	90%

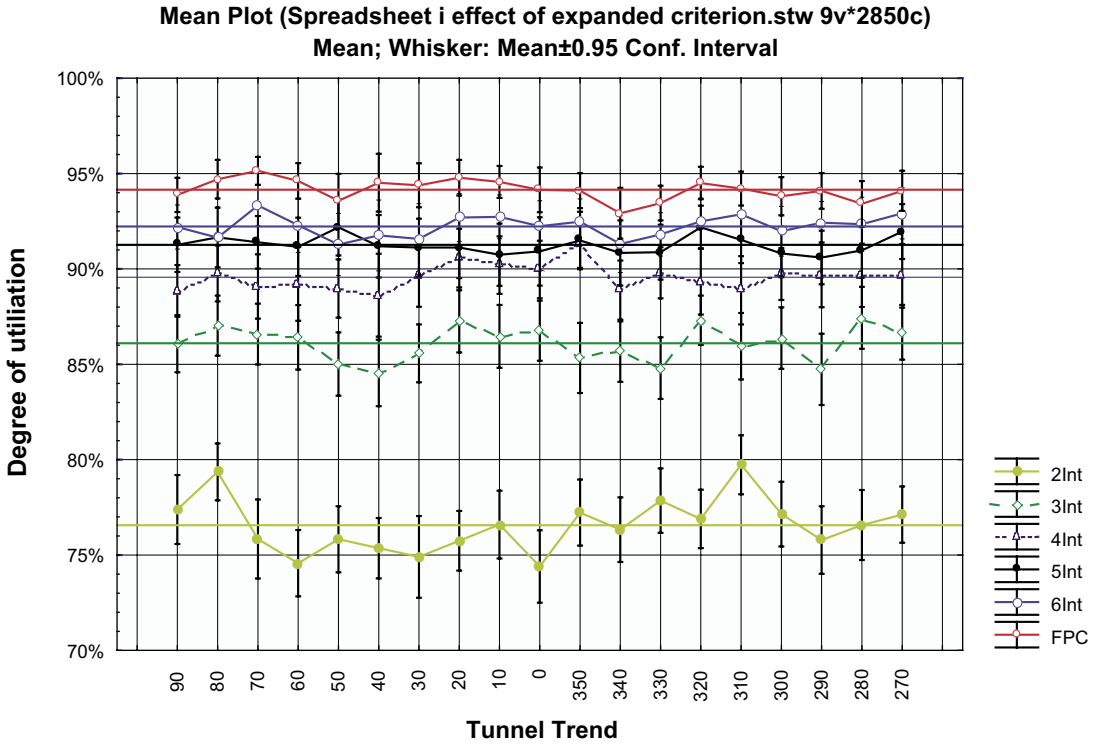

Figure 7-3. *Difference in degree of utilisation using different number of deposition hole intersections for EFPC.*

8 Summary and conclusions

The consequence of using the Full Perimeter Criterion (FPC) has been quantified in terms of degree of utilisation which was judged reasonable. The degree of utilisation is higher in Forsmark as compared to Laxemar due to, mainly; the latter's higher intensity of the steep fracture sets in the studied size interval.

The FPC was found insufficient to detect all potentially discriminating fractures. It needed to be complemented and we defined a new criterion, EFPC, to also address large fractures in the immediate vicinity of the tunnel, which remain undetected by tunnel mapping. We here proposed a criterion consisting in discriminating also all fractures that intersect 5 or more canister positions. The use of EFPC decreased the degree of utilisation further, though we still judge it to be reasonable.

A substantial reduction of unsuitable canister positions is obtained with the application of the suggested criterion. It is also noted that a substantial number of fractures are erroneously marked as being discriminating, thus implying a 'cost' in terms of degree-of-utilisation. Using the Forsmark and Laxemar repository layouts as example, we showed that site specific application of the criterion combined with respect distances significantly increased the efficiency of the criterion to a presumably acceptable level; only 3 canister positions in Laxemar and 4 positions in Forsmark out of 6,000 were erroneously marked as "approved" whereas around 182 and 98 deposition holes, for Laxemar and Forsmark respectively, are erroneously accepted if the criterion is not applied. The 'cost' in this case is an increase in the required total deposition tunnel length of 4.7 km and 3.2 km for Laxemar and Forsmark respectively (using 6 m spacing). As the fractures are cautiously assumed to be completely anonymous features possessing no indications of their size, we anticipate that the majority of the erroneously approved positions will in fact be detected if the criterion is linked to an adequate, qualitative judgement based on site understanding and underground information.

Despite the uncertainties in the DFN models, we found the results of the simulations sufficiently encouraging to recommend the Full Perimeter Criterion and it's expansion, EFPC, as a method to identify potentially discriminating fractures.

9 Acknowledgements

This report greatly benefited from the meticulous reading and quest for clarity by Martin Stigsson who also assisted eagerly with computational wizardry, a never ending enthusiasm and some independent checks of the simulation results. Allan Hedin is thanked for many valuable improvements of this work and with whom we have had numerous stimulating discussions on the matter. Allan also provided algorithms for computing “epsilon” and an analytical benchmark for FPI. Harald Hermansson is warmly thanked for his thorough review of the equations and the suggestions of improvements of the Matlab codes.

10 References

Börgesson L, Johannesson L-E, Hernelind J, 2003. Earthquake induced rock shear through a deposition hole. Effect on the canister and the buffer. SKB TR-04-02, Svensk Kärnbränslehantering AB.

Devroye L, 1986. Non-Uniform Random Variate Generation, Springer-Verlag. New York.

Fälth B, Hökmark H, 2006. Seismically induced shear displacement on repository host rock fractures. Results of new dynamic discrete fracture modeling. R-06-48, *in prep*, Svensk Kärnbränslehantering AB, Stockholm, Sweden.

Hagros A, McEwen T, Anttila P, Äikäs K, 2005. Host rock classification. Phase 3: proposed classification system (HRC-system). Posiva Working Report 2005-07, Posiva Oy Olkiluoto Finland.

Hedin A, 2005. An analytic method for estimating the probability of canister/fracture intersections in a KBS-3 repository. SKB R-05-29, Svensk Kärnbränslehantering AB.

Hermanson J, Fox A, La Pointe P R, Forssberg O, 2005. Statistical model of fractures and deformation zones. Preliminary site description, Laxemar sub-area, Version 1.2. SKB R-05-45, Svensk Kärnbränslehantering AB.

La Pointe P R, Olofsson I, Hermanson J, 2005. Statistical model of fractures and deformation zones for Forsmark. Preliminary site description Forsmark area – version 1.2. SKB R-05-26, Svensk Kärnbränslehantering AB.

Munier R, Hökmark H, 2004. Respect distances. Rationale and means of computation. SKB R-04-17, Svensk Kärnbränslehantering AB.

Scneider P, Eberly D, 2003. Geometric tools for computer graphics, Morgan Kaufmann Publishers. San Fransisco, USA, ISBN 1-55860-594-0.

SKB, 2002. Djupförvar för använt kärnbränsle. Anläggningsbeskrivning – Layout E. Schaktalternativ med ett driftområde. SKB R-02-19, Svensk Kärnbränslehantering AB.

SKB, 2004. Deep repository. Underground design premises. Edition D1/1. SKB R-04-60, Svensk Kärnbränslehantering AB.

SKB, 2005a. Preliminary safety evaluation for the Forsmark area. Based on data and site descriptions after the initial site investigation stage. SKB TR-05-16, Svensk Kärnbränslehantering AB.

SKB, 2005b. Preliminary safety evaluation for the Simpevarp subarea. Based on data and site descriptions after the initial site investigation stage. SKB TR-05-12, Svensk Kärnbränslehantering AB.

SKB, 2005c. Preliminary site description. Forsmark area – version 1.2. SKB R-05-18, Svensk Kärnbränslehantering AB.

The MathWorks Inc, 2006. MatLab 7. 7.2.0.232 (R2006a). The MathWorks Inc. 3 Apple Hill Drive, Natick, MA 01760-2098, USA. www.matlab.com.